Data assimilation and bathymetric inversion in a two-dimensional horizontal surf zone model

G. W. Wilson,[1] H. T. Özkan-Haller,[1] and R. A. Holman[1]

Received 18 March 2010; revised 30 July 2010; accepted 1 October 2010; published 21 December 2010.

[1] A methodology is described for assimilating observations in a steady state two-dimensional horizontal (2-DH) model of nearshore hydrodynamics (waves and currents), using an ensemble-based statistical estimator. In this application, we treat bathymetry as a model parameter, which is subject to a specified prior uncertainty. The statistical estimator uses state augmentation to produce posterior (inverse, updated) estimates of bathymetry, wave height, and currents, as well as their posterior uncertainties. A case study is presented, using data from a 2-D array of in situ sensors on a natural beach (Duck, NC). The prior bathymetry is obtained by interpolation from recent bathymetric surveys; however, the resulting prior circulation is not in agreement with measurements. After assimilating data (significant wave height and alongshore current), the accuracy of modeled fields is improved, and this is quantified by comparing with observations (both assimilated and unassimilated). Hence, for the present data, 2-DH bathymetric uncertainty is an important source of error in the model and can be quantified and corrected using data assimilation. Here the bathymetric uncertainty is ascribed to inadequate temporal sampling; bathymetric surveys were conducted on a daily basis, but bathymetric change occurred on hourly timescales during storms, such that hydrodynamic model skill was significantly degraded. Further tests are performed to analyze the model sensitivities used in the assimilation and to determine the influence of different observation types and sampling schemes.

Citation: Wilson, G. W., H. T. Özkan-Haller, and R. A. Holman (2010), Data assimilation and bathymetric inversion in a two-dimensional horizontal surf zone model, *J. Geophys. Res.*, *115*, C12057, doi:10.1029/2010JC006286.

1. Introduction

[2] Many nearshore circulation models utilize the depth- and wave-averaged equations of motion, coupled with a "wave driver" for transfer of momentum from incident gravity waves to surf zone currents. When validating these models (i.e., assessing their ability to match observations), one must consider two sources of error: mis-specification of physical processes in the model, and errors in model inputs, namely the underlying bathymetry and boundary conditions. Here we will refer to these as "process error" and "input error", respectively.

[3] The majority of previous studies [e.g., *Longuet-Higgins*, 1970; *Thornton and Guza*, 1986; *Reniers and Battjes*, 1997] have focused on minimizing process error, leading to improved parameterizations and empirical calibrations now standard in nearshore models. Meanwhile, the potential role of input error is often acknowledged but tends to be difficult to quantify, let alone to correct. An important example, which is the focus of this paper, is the presence of bathymetric uncertainty when modeling surf zone currents.

[4] Bathymetric input error may appear in various forms. In the extreme case, where the bathymetry has not been measured, one is forced to assume some reasonable beach shape for the model. Even when measurements are available, they are subject to instrument error. Spatial undersampling may not resolve high wave number bathymetric features [*Plant et al.*, 2002], and the resulting spatial smoothing may affect model outputs [*Plant et al.*, 2009]. Temporal undersampling may also occur, as beach changes occur on daily or even hourly time scales. In field situations, these various sources of bathymetric input error may be as important as process error as constraints on model accuracy.

[5] In this study, we address the issue of bathymetric input error from two perspectives. First, we seek to quantify the sensitivity of the model to errors in bathymetry. Second, at the same time, we evaluate a method for indirectly correcting bathymetric errors, by incorporating in situ measurements of waves and currents. These two perspectives encompass data assimilation and bathymetric inversion.

[6] In previous data assimilation efforts, *Feddersen et al.* [2004] used a variational approach [*Bennett*, 2002], deriving adjoint equations for a surf zone model involving linearized alongshore-uniform dynamics, to assimilate pressure and bi-directional current (PUV) measurements on a natural beach. *Kurapov et al.* [2007] extended this approach to the nonlinear two-dimensional horizontal (2-DH) time-dependent equations, and used the process of nonlinear shear

[1]College of Oceanic and Atmospheric Sciences, Oregon State University, Corvallis, Oregon, USA.

0148-0227/10/2010JC006286

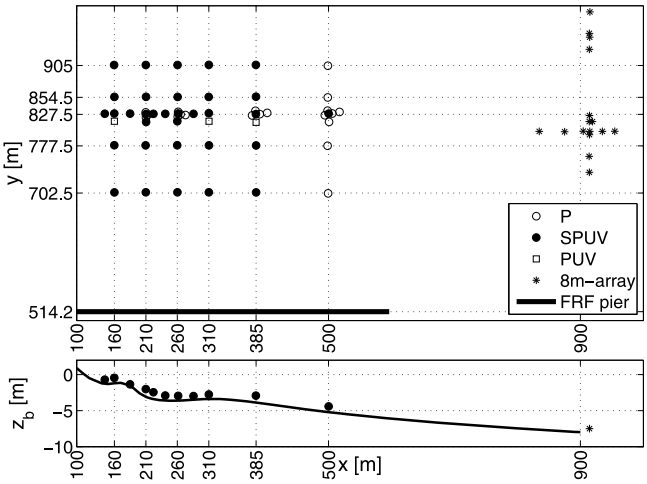

Figure 1. (top) Plan view map of observational array. (bottom) Side view, with depth transect from 22 September survey, showing typical bathymetric profile and sensor positions in water column. Still water level ranged from –0.5 to 1.5 m NGVD during the experiment.

instability in alongshore currents [*Slinn et al.*, 1998] as a test bed for variational data assimilation. Both these studies focused on model sensitivity in the form of forcing errors, which we would characterize as process error. *Feddersen et al.* [2004] also considered sensitivity to the bottom friction coefficient, i.e., input error.

[7] Regarding the topic of surf zone bathymetric inversion, the majority of previous studies have focused on the technical challenge of observing surface wave properties, which are often related to water depth using simple physical models. For instance, previous studies have estimated bathymetry using the linear wave dispersion relationship [*Stockdon and Holman*, 2000], the nonlinear wave dispersion relationship [*Catalan and Haller*, 2007], or wave refraction [*Splinter and Holman*, 2009]. Wave breaking dissipation proxies have also been used in combination with empirical models [*Aarninkhof et al.*, 2005] to infer bathymetric changes.

[8] Recently, *VanDongeren et al.* [2008] have applied data assimilation techniques to the problem of bathymetric inversion, providing a fresh perspective on this long-standing problem. Their method employs a sequential least squares estimator, which assimilates multiple remote sensing (video and radar) wave observations. While not as sophisticated as the variational schemes of *Feddersen et al.* [2004] or *Kurapov et al.* [2007], their technique stems from a comparable approach. Adjoint equations are derived, in this case, from simple localized models for the observed physical processes. Spatial covariance is neglected (although this may be unimportant for the spatially-dense observations being considered), and temporal covariance is approximated empirically. Despite these simplifications, their results show the most robust and reliable bathymetric inverse to date. This reliability stems from the important step of acknowledging data errors as well as model errors, and covariances thereof, in order to form a statistically optimal estimate.

[9] The present work is conceptually similar to that of *VanDongeren et al.* [2008], but with some key differences. First, our method quantifies model sensitivity using statistical, rather than analytical, means. This facilitates the assimilation of arbitrary geophysical variables, without having to compute their derivatives with respect to depth (i.e., adjoint equations). Second, we incorporate spatial covariance, and hence can compute nonlocal corrections based on local in situ measurements. Finally, we put special emphasis on bathymetric sensitivity and its role in the inversion problem.

[10] The paper is organized as follows: section 2 introduces the in situ data set. Section 3 presents the data assimilation methodology: the parameter estimation scheme, the hydrodynamic model, and the technique used to represent bathymetric uncertainty. Section 4 gives examples of the application of that methodology to field data. Sections 5 and 6 summarize and discuss the results, and give conclusions.

2. Observations

[11] In this study, we will use a subset of the data collected during the SandyDuck '97 (SD97) experiment (Duck, NC); Figure 1 shows the experimental layout. Between 22 September and 31 October, the U.S. Army Corps of Engineers Field Research Facility (FRF) conducted 38 daily bathymetric surveys in the region shown (except for 19 October), using the CRAB survey vehicle [*Birkemeier*, 1984] to collect multiple across-shore transects of bathymetry spaced 25–50 m apart. These surveys were interpolated onto a regular grid with 5 m and 10 m spacing in the across-shore and alongshore directions, respectively, using a quadratic loess filter [*Plant et al.*, 2002] with interpolation filter length scales of 200 m in the alongshore direction, and 5 m in the across-shore direction. Additional bathymetry was incorporated from larger-scale surveys conducted on 16 September and 23 October, such that the total model domain was $0 \le x \le 900$ m and $0 \le y \le 1000$ m; the detailed daily surveys were stitched on top of the larger-scale bathymetry using weighted interpolation, i.e.,

$$h = wh_0 + (1 - w)h_1, \tag{1}$$

where h_0 is the larger-scale bathymetry, h_1 is the detailed minigrid bathymetry, and w is a weighting function which ramps from 0 to 1 over 50 m at each edge (using a tanh shape). Herein, Figures 1, 4, 5, 7, 9–11, 13, and 14 will present bathymetric data in terms of distance from the National Geodetic Vertical Datum (NGVD) to the seafloor, or z_b; that is, $h = -z_b + z_t$, where z_t is the still water level (which changes with time due to tide and large-scale surge).

[12] An offshore array of 15 bottom-mounted pressure gages (labeled "8 m array" in Figure 1 [*Long*, 1996]) provided frequency-directional wave spectra at 3 h intervals, which are used to specify the offshore boundary for the wave model (section 3.3). When the model time is not centered on a 3-h collection time, a time-interpolation is applied using the scheme described in the SWAN wave model user manual (www.wldelft.nl).

[13] In situ measurements from sonar altimeters, pressure gages, and bidirectional current meters (SPUV) were provided

at the locations shown in Figure 1 [*Elgar et al.*, 2001]. These were processed to obtain the significant wave height H_{mo} (17 min intervals), time-averaged currents (17 min intervals), and estimated depths (3 h intervals). The depth measurements were further processed by comparing to the daily bathymetric surveys; offsets which persisted for five or more days were removed from the sonar altimeter data, in cases where the offset was significant (using Welch's t test for significance of bias, with $n \geq 5$ and $p < 0.05$) and the correlation was significant and positive ($p < 0.05$, $r > \sqrt{0.1}$). These corrections were typically small (less than 20 cm) and in deep water (depths greater than 3 m). Agreement with the CRAB surveyed depths was otherwise excellent (root-mean square difference was 7.3 cm).

3. Methodology

[14] In this section, we outline a methodology for assimilating data and generating bathymetric inversions based on point observations of wave height and alongshore current. As a general overview, the method involves the following steps:

[15] 1. Generate an ensemble h^f (f for "forecast," following the standard notation) consisting of N realizations of bathymetry (in our application, $N = 150$). The distribution of the ensemble should be representative of prior knowledge and uncertainty (section 3.2).

[16] 2. Apply the hydrodynamic numerical model (section 3.3) to each of the N bathymetric ensemble members, assuming other inputs are perfect (e.g., wave spectrum at offshore boundary), and store the output.

[17] 3. Compute the sample mean and covariance from the ensemble of modeled fields.

[18] 4. Generate an updated (posterior) state ψ^a (a for "analysis," equation (3)), which includes bathymetry, wave height, currents, and calculate the posterior uncertainty $C^a_{\psi\psi}$ (equation (5)).

[19] We note this methodology is not particularly new or novel: *Mourre et al.* [2004] have previously applied ensemble-based methods (steps 1–3) to examine bathymetric sensitivity in a regional ocean model. The equations for optimally updating the model (step 4) are following a vast and ongoing literature on data assimilation using ensemble-based methods, for example the Ensemble Kalman Filter (EnKF) (see *Evensen* [2006] on which the present method is largely based, as well as references therein). The following section reviews the existing methodology, as it applies to the unique problem studied here: nearshore bathymetric sensitivity and inversion.

3.1. Theory for Bathymetric Inversion

[20] To begin, we define some notation which will be useful in what follows. Suppose, for simplicity, we are dealing with a single observable v. In later sections we will in fact observe and assimilate two variables, alongshore current and wave height, but the extension is straightforward: simply augment v with H_{mo}. We are also given a model, $v = G(h)$, which makes predictions of v on a discrete spatial grid, given the water depth h. Here we have assumed the model (including all boundary conditions and inputs other than h) is "perfect," so the error of the model prediction is due only to errors in h. To that point, we define the model input bathymetry $h = h^t + p$, where h^t is the true bathymetry. When the error p is included in the model input, the resulting prediction is $v = G(h^t + p) = v^t + q$.

[21] Our goal is to obtain an optimal estimate of the true field on the model grid, $v^t = G(h^t)$, given a set of K observations which are themselves subject to some error ε, $d = Lv^t + \varepsilon$. Here L is a measurement operator, in our case simply a matrix which linearly interpolates from the gridded field to the measurement locations. We define the optimal posterior estimate ψ^a as the one which minimizes the following cost function:

$$\mathcal{J}[\psi] = \left(\psi - \psi^f\right)^T W_{\psi\psi}\left(\psi - \psi^f\right) + (d - Lv)^T W_{dd}(d - Lv), \tag{2}$$

where $\psi = [v^T, h^T]^T$ is a state variable in which v is augmented with h (note v and h should each be treated as $M \times 1$ vectors, where M is the total number of model grid points), ψ^f corresponds to a prior estimate for v and h, and $W_{\psi\psi}$ and W_{dd} are positive-definite weighting matrices.

[22] Note that $\mathcal{J}$ contains a "model" part and a "data" part: the model part says the posterior state should not stray too far from the prior (hence, it retains physics from the model solution), and the data part says the posterior should match closely with observations. If $W_{\psi\psi} \gg W_{dd}$ ("perfect prior") the posterior solution is just the prior ψ^f, and if $W_{dd} \gg W_{\psi\psi}$ ("perfect data") the posterior solution is an exact interpolation of the data d. Clearly, the perfect-prior assumption ignores the information contained in the observations; the perfect data assumption, on the other hand, can lead to interpolation of observation noise. Hence, a central challenge of data assimilation is to find the correct balance between these two extremes by correctly choosing the weights W. In some cases, it is useful to "hedge" the estimate toward the prior, for instance if there is a possibility of instrument malfunction. In other cases, the observations are known to be very accurate and a perfect-data assumption is valid.

[23] It can be shown [*Evensen*, 2006; *Bennett*, 2002] that the solution ψ^a which minimizes $\mathcal{J}$ is given by

$$\psi^a = \psi^f + C_{\psi\psi}L_a^T\left(LC_{vv}L^T + C_{dd}\right)^{-1}\left(d - Lv^f\right), \tag{3}$$

where $L_a = [L, 0^{K\times M}]$ is an augmented measurement operator for extracting v from ψ, and $C_{\psi\psi}$ and C_{dd} are the inverse of the weights $W_{\psi\psi}$ and W_{dd}. Specifically, $C_{\psi\psi}$ has the following structure:

$$C_{\psi\psi} = \begin{pmatrix} C_{vv} & C_{vh} \\ C_{hv} & C_{hh} \end{pmatrix} \tag{4}$$

By choosing $C_{\psi\psi}$ as the covariance, equation (3) gives the maximum likelihood estimator for Gaussian statistics.

[24] At this point equation (3) can be viewed as a general solution, and the problem is reduced to specifying $C_{\psi\psi}$ based on properties of the model (C_{dd} is typically specified as a diagonal matrix whose elements are the observation error variances). The simplest approach is to define $C_{\psi\psi}$ a priori without reference to the model itself. A more attractive approach, which recognizes the intrinsic properties of the model, is the method of representer expansions [*Bennett*, 2002]. That method requires the specification of C_{hh}, but

uses the model (via adjoint equations, which must be derived) to obtain the corresponding C_{vh} and C_{vv}. *Feddersen et al.* [2004] and *Kurapov et al.* [2007] used representer expansions, except their goal was to correct forcing and/or bottom friction, not bathymetry. *VanDongeren et al.* [2008] used a hybrid approach, where C_{vh}, C_{vv}, and C_{hh} were assumed a priori to be diagonal matrices (hence the correction is localized), but are related to one another by a physical model. In our application, we use an ensemble-based methodology, described next.

[25] The crux of ensemble-based methods (e.g., the Ensemble Kalman Filter [*Evensen*, 2006]) is that $C_{\psi\psi}$ is approximated by the sample covariance of a representative ensemble ψ_i^f, $i = 1, 2, \ldots, N$. This ensemble is generated by applying the forward model G to an ensemble of inputs h_i^f, drawn from a statistical distribution specified by some reasonable C_{hh} (see section 3.2). In the update step, one applies equation (3) to each member of the ensemble (each time treating $\psi^f = \psi_i^f$) to obtain the posterior members ψ_i^a. The sample mean of ψ_i^a is interpreted as the posterior state estimate, and the sample covariance provides a posterior estimate of uncertainty (under a Bayesian interpretation), given by

$$C_{\psi\psi}^a = C_{\psi\psi} - C_{\psi\psi}L_a^T\left(LC_{vv}L^T + C_{dd}\right)^{-1}L_aC_{\psi\psi}. \tag{5}$$

3.2. Prior Bathymetric Ensemble

[26] Section 3.1 showed that the problem estimating v and h, based on observations d, hinges on the specification of the bathymetric covariance matrix C_{hh}. In our application, we do not explicitly define C_{hh}, but instead we construct an ensemble of bathymetric realizations h_i, in such a way as to represent the spread of potential bathymetric error to the best of our knowledge. C_{hh} is then approximated by the sample covariance of that ensemble.

[27] We assume the dominant bathymetric error, in this context, is due to integrated sediment transport between bathymetric surveys (instrument error is also present, but we have attempted to minimize its impact using loess interpolation, see section 2). Hence, the reasonable spread of bathymetric realizations should be constrained by measurements (survey data from the recent past/future). We must also limit the ensemble to realistic bathymetries: perturbations around the prior mean h must not include physically unrealistic shapes or features. To that end, we seek realizations on the state-space where bathymetric change naturally occurred throughout the experiment. We approximate this space by applying an empirical orthogonal functions (EOF) decomposition to the complete set of interpolated bathymetric surveys over the entire experiment. For a particular bathymetric ensemble, the prior mean loadings are set to the time-mean observed loadings from a 72 h period surrounding the target time. The prior standard deviation of loadings is set equal to the range of loadings observed over the same time period.

[28] Figure 2 shows the leading modes of the EOF decomposition, and their corresponding percent of variance. The first mode represents full-domain surveyed change (only two full-domain surveys were conducted); subsequent modes show increasing detail mostly focused on the dynamics of the inner bar at $x \approx 150$ m in the minigrid domain (defined as 550 m $\le y \le$ 1000 m). For instance, the across-shore position and width of the inner bar is mainly determined by EOF modes 2 and 3.

3.3. Forward Model

[29] Once the bathymetric ensemble is specified, we must generate the corresponding ensemble of observables v_i^f, which involves applying a forward model to each ensemble member h_i^f. Here we use the freely-available code shoreCirc (version 2.0, [*Svendsen et al.*, 2000]) to solve the depth-integrated and wave-averaged equations of motion for arbitrary bathymetry. These comprise the momentum equation,

$$\frac{\partial Q_\beta}{\partial t} + \frac{\partial}{\partial x_\alpha}\left(\frac{Q_\alpha Q_\beta}{(h+\eta)}\right) = -g(h+\eta)\frac{\partial \eta}{\partial x_\beta} - \frac{1}{\rho}\left(\tau_\beta^s - \tau_\beta^b + \tau_\beta^M + \tau_\beta^{\mathrm{Q3D}}\right) - \frac{1}{\rho}\frac{\partial S_{\alpha\beta}}{\partial x_\alpha}. \tag{6}$$

and the conservation of mass equation,

$$\frac{\partial \eta}{\partial t} + \frac{\partial Q_\alpha}{\partial x_\alpha} = 0, \tag{7}$$

where α and β are dummy indices for horizontal coordinates (summation is implied over repeated indices). In these equations, Q is the depth-integrated volume flux, h is the still water depth, and η is the wave-averaged water surface elevation. We define the depth-averaged across-shore and alongshore current as $u = (Q_x - Q_{wx})/(h + \eta)$ and $v = (Q_y - Q_{wy})/(h + \eta)$, respectively, where Q_w is the contribution to volume flux from waves (approximated using linear wave theory). τ^s and τ^b are surface and bottom shear stresses, τ^M is a nondissipative momentum mixing, τ^{Q3D} represents "quasi-3-D" mixing [*Svendsen and Putrevu*, 1994], and S is the radiation stress tensor [*Longuet-Higgins and Stewart*, 1964]. Details of the parameterizations of the various terms can be found in the shoreCirc manual (http://chinacat.coastal.udel.edu/programs/nearcom). Default values for physical constants were used throughout, except for the bottom friction coefficient f_w which was specified as 0.0053 (cf. [*Feddersen and Guza*, 2003]). We employ no-flux shoreline boundary conditions (the shoreline is defined as $h = 0.05$ m), and radiation offshore boundary conditions. The lateral boundaries are treated as periodic, where a 300 m artificial buffer zone is added to enforce periodicity in the model inputs. The equations are solved on a mesh with (Δx, Δy) = (5, 10) m, and time step $\Delta t = 0.18$ s.

[30] To define the time-independent model operator G, equations (6) and (7) are integrated from rest to steady state. Shear instability of the alongshore current [*Bowen and Holman*, 1989] did not occur for the conditions tested here, except if the quasi-3-D terms were turned off, similar to the results of *Zhao et al.* [2003]. Hence, the steady state flow corresponds to a single snapshot of the final model state.

[31] To compute the radiation stress gradients due to wave motion, as well as other wave-related quantities which appear in equation (6) via parameterizations, we use another

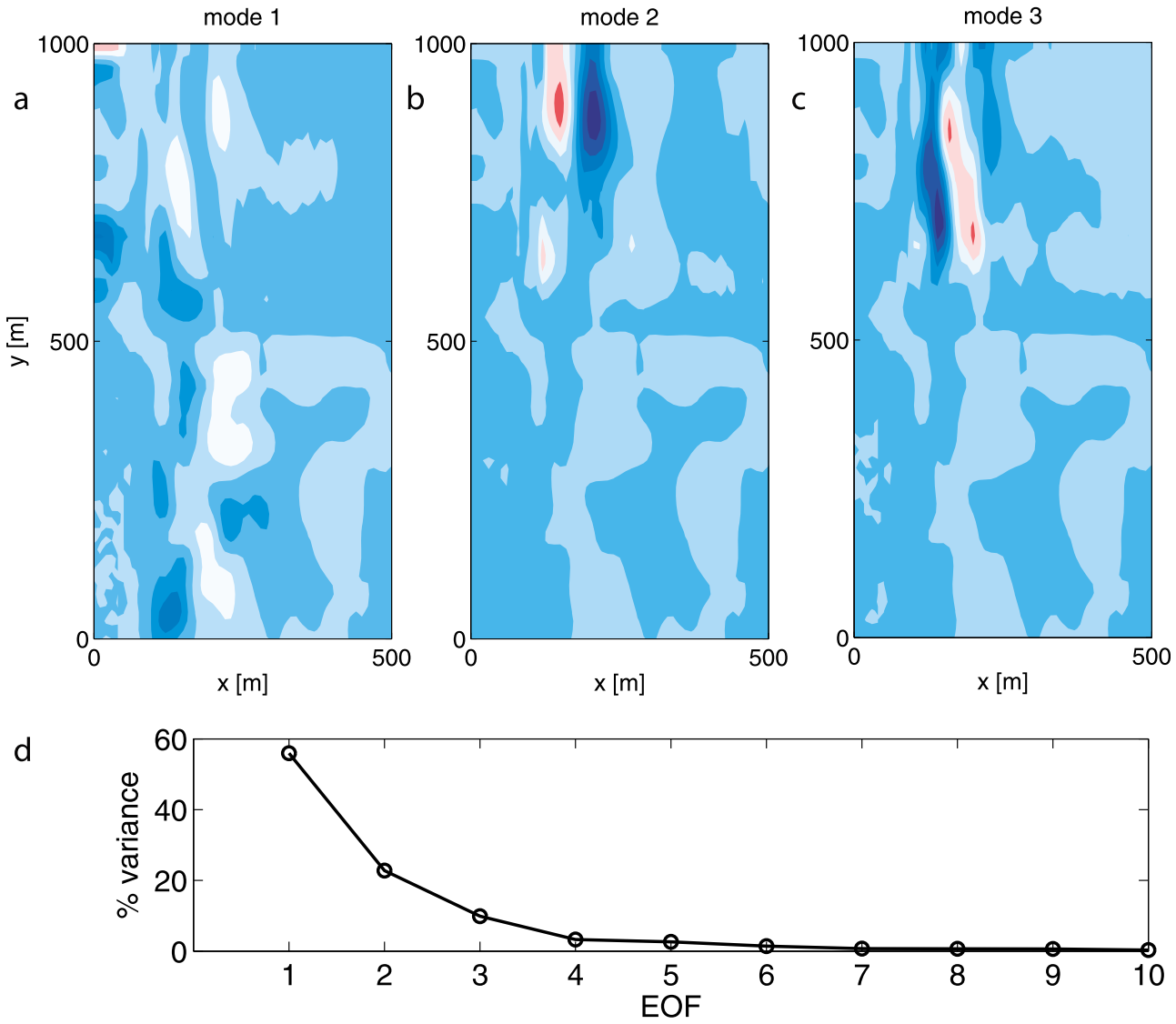

Figure 2. (a–c) Leading modes in bathymetric EOF decomposition (normalized to unit variance). (d) Percentage of total variance for leading 10 modes of bathymetric EOF decomposition.

freely available code, SWAN [*Booij et al.*, 1999]. SWAN solves the spectral wave action-balance equation [*Mei*, 1983], and thus predicts the full-field wave spectral transformation. The model is initialized with measured wave frequency-directional spectra at the offshore boundary (see section 2). We include the effect of the wave roller, a mass of aerated water which travels on the face of breaking waves, using the formulation of *Reniers and Battjes* [1997] [also *Reniers et al.*, 2004; *Ruessink et al.*, 2001]. We neglect interaction between the waves and the wave-averaged velocities.

[32] The accuracy of the above model, although assumed perfect for the purposes of developing the data assimilation methodology, is in fact limited by many underlying assumptions about physical processes. In practice, it is very difficult to quantify the process model accuracy, except in very controlled laboratory conditions, because of the simultaneous presence of model input errors (the focus of the present work). An example of such a controlled validation is provided by *Haas et al.* [2003], who applied shoreCirc to simulate a laboratory rip current flow. In that study, shoreCirc was shown to reproduce the broad features of the 2-DH flow, while smaller-scale flow details were shown to be influenced by errors in the bathymetric input. They also found the accuracy of shoreCirc to be comparable to that of a wave-resolving Boussinesq model.

[33] The present model is also known to be as accurate as other available 2-DH numerical codes under comparable field conditions. *Wilson* [2009] performed a validation of the present model for 455 h of the SD97 field experiment, and found RMS errors of order 5–15 cm for H_{mo} and 10–20 cm/s for v (larger errors occurring closer to shore). Similar values have been reported by *Ruessink et al.* [2001] (for a 1-DH model), and *Morris* [2001] and *Hsu et al.* [2006] (for 2-DH models), among others. Hence, the present model setup is

considered representative of the state of the art for depth-integrated wave-averaged nearshore prediction.

3.4. Observational Error Estimates

[34] We assume observation error standard deviations of 6.7 cm/s in alongshore current, and 7.0 cm in significant wave height. These values encompass errors of measurement (instrument noise), as well as so-called representation errors (the two are added in quadrature). The former are due to practical issues of data collection and quality, while the latter are due to the fact that what the model predicts is not strictly comparable to what is measured.

[35] Measurement error standard deviation for v has been estimated using laboratory and field calibration [*Feddersen and Guza*, 2003] as $(\sigma_0^2 + (\alpha|v|)^2)^{1/2}$, where $\sigma_0 = 5$ cm/s, and $\alpha = 0.05$. For the present case, $|v| \sim 0.75$ m/s, and we therefore assume a measurement error standard deviation of 6.25 cm/s for v.

[36] To obtain an estimate of measurement error for H_{mo} during SD97, we have compared measurement differences for sensors placed less than 4.5 m apart in the alongshore direction and less than 0.55 m apart in the across-shore direction (four sensor pairs passed this criteria, located from $x = 210$ m to $x = 261$ m). The standard deviation of measurement differences, based on over 2500 h of data, ranged from 3.6 cm to 6.3 cm. Values were increased for sensors closer to shore, and for increasing offshore wave height. Hence we assume a (conservative) measurement error standard deviation of 6.5 cm for H_{mo}.

[37] Several potential sources of representation error exist in the present model. One example is the fact that the measurements were collected at a particular water depth, whereas the model predicts depth-averaged flow. Further, the measurements may have been sampled during slowly-varying conditions (such that time averaging of observational data does not suffice to remove the variability), or may even be unsteady [*Bowen and Holman*, 1989], whereas the model predicts the steady state waves and flow which would occur under static conditions. The treatment of representation error is not trivial, and is the subject of ongoing research [e.g., *Oke and Sakov*, 2007, and references therein]. Here we simply assume a constant, spatially-uniform contribution to the observational error, of 2.5 cm/s for v and 2.5 cm for H_{mo}. We have tested different values of total observational error, and find no qualitative change in the posterior solution.

3.5. Underlying Assumptions and Optimality

[38] Several assumptions underlie the derivation of equation (3), which should be kept in mind when applying the method. Importantly, we have assumed that the model is "perfect," in the sense that if the true inputs h^t were known, the output $v^t = G(h^t)$ would be exact. This assumption pertains to physical processes in the model, as well as boundary conditions: for the present application, the latter is important because the offshore boundary condition (an input wave spectrum) is itself derived from measurements. While this effect may be reduced at locations far from the boundary (i.e., the inner surf zone), it is likely not negligible.

[39] Another factor in the interpretation of equation (3) as an "optimal" solution is the assumption of Gaussian statistics. In our case, the model operator G is nonlinear, hence the statistics are not likely to be Gaussian. Therefore, we will avoid the use of the term "optimal" in describing the posterior estimates. Instead, we interpret the results as a least squares estimate, based on approximate model statistics.

[40] Finally, the quality of the posterior estimate is conditioned by the quality of the prior statistics. Specifically, one must define an appropriate prior mean/covariance for the bathymetry, and a reasonable error model for the observations. The present results are based on rational and well-defined estimates of those statistics, as described above, but these estimates are still subjective, to some degree. In practice, we have found the quality of the posterior to be degraded if the prior statistics are not carefully defined, and this may be unavoidable in the absence of extensive observational data. An attractive extension of the present method would be to include time-evolution in the ensemble statistics, as in the sequential method of *VanDongeren et al.* [2008]. Using that approach, the prior statistics are only specified once, and are continually updated whenever measurements become available (using equations (3) and (5); this is the Ensemble Kalman Filter, [*Evensen*, 2006]). Such an extension is highly recommended for future application of the present method.

[41] The above caveats underscore the need for cross-validation when applying the present method. Therefore, in the following, we first show the applicability and skill of the method before using it to assess the sensitivity of modeled circulation to bathymetric uncertainty.

4. Results

[42] In this section, we demonstrate the ability of the statistical inverse method to estimate bathymetry, in a situation where it was not possible to conduct a bathymetric survey. Our primary example case is for 1530 EST on 20 October, for which the dynamics are 2-DH. This time was selected due to its interesting morphodynamic setting, the presence of strongly 2-DH flow features, and a low rate of instrument malfunctions in shallow water. Before moving to this more-complex 2-DH case, however, we will present a 1-DH case study from the same day, at 1130 EST. The 1-DH case will serve to introduce important conceptual topics related to the assimilation methodology.

4.1. Physical Setting

[43] The conditions surrounding 20 October were strongly influenced by the passage of a Nor'easter storm, which peaked during the hours 1600–1900 EST on 19 October. The measured significant wave height (at 8 m depth) during the storm was 3.4 m. Somewhat less-energetic conditions continued throughout the day on 20 October. Figure 3 summarizes the observed conditions.

[44] No bathymetric survey was conducted on 19 October due to dangerous conditions. Complete minigrid surveys were conducted, however, on 18 October, 0600–1340 EST, and 21 October, 0550–1530 EST. Also, a limited survey was conducted on 20 October, 0630–1040 EST. Figure 4 summarizes these bathymetric observations. The sequence of surveyed bathymetries illustrates the speed with which bathymetric change occurred in the days surrounding the storm. The surveyed transects suggest changes in across-shore bar profile, alongshore variability, or both (the exact

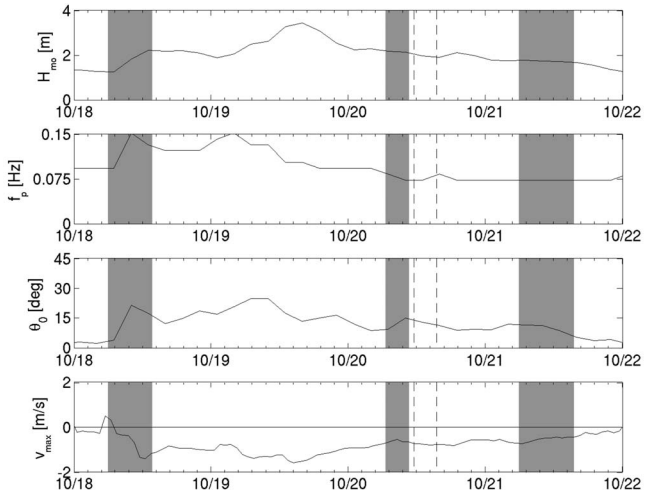

Figure 3. Conditions observed for the period from 18 to 21 October during the SD97 experiment: offshore significant wave height H_{mo}, peak frequency f_p, mean wave angle θ_0 [*Kuik et al.*, 1988] (positive is from the north), and maximum alongshore current in SPUV array v_{max} (positive is toward the north). Shaded regions represent times when bathymetric surveys were being performed (see Figure 4). Dashed lines correspond to 20 October, 1130 EST and 1530 EST (sections 4.2 and 4.3).

morphodynamics may not be resolved by the surveys). This rapid bathymetric change, combined with the paucity of survey data on 19 and 20 October, makes specification of model bathymetry quite difficult for the target model times, which can be between survey times. Temporal interpolation from surveys would be a questionable approach, as the surveys, as well as the sonar altimeters, suggest a nonmonotonic change through time. Hence the present method has practical relevance, because it makes use of additional time-resolved measurements (wave height, velocity) to improve the bathymetric estimate.

[45] The observed flow during the 19 October storm was alongshore uniform (1-DH) and reached speeds of up to 1.6 m/s. Over the course of the day of 20 October, conditions changed such that the observed flow was weaker, and exhibited alongshore-nonuniformity (2-DH). Indeed, as we will see in later sections, assimilation of data on 20 October, 1530 EST, leads to a 2-DH posterior model state. However, at earlier times on 20 October, particularly at high tides, the observed (and posterior estimated) flow was closer to 1-DH. Next, we study such a case, 1130 EST, as a simple dynamical setting in which to introduce the present method.

4.2. Conceptual Interpretation: A 1-DH Case Study

[46] In this section, we run the forward model assuming $\partial/\partial y = 0$ in the governing equations, using as the bathymetry a single transect y = 828 m from the 2-DH bathymetric ensemble (observational data are taken from the same transect). The assumption of 1-DH dynamics is only approximately valid, here. For instance, v measured on the transect x = 160 m varied from –45 cm/s (y = 704 m) to −70 cm/s (y = 816 m) (no other sensors were functioning at the time on x = 160 m). On the transect x = 210 m (five sensors), v varied from −68 cm/s (y = 906 m) to −50 cm/s (y = 816 m), with mean −59 cm/s and standard deviation 7.1 cm/s. However, neither the measurements nor a 2-DH assimilation indicated any strongly 2-DH features such as rip currents. Moreover, our purpose in this section is to elucidate the mechanics of the assimilation in the context of simple 1-DH model dynamics. Cross-validation using more-accurate 2-DH dynamics will be taken up in later sections.

[47] Figure 5 shows the prior and posterior predictions of bathymetry, velocity, and wave height, compared to measurements. The prior bathymetry does not include a sharp nearshore bar, as was measured by the sonar altimeters, and confirmed by a nearby CRAB survey transect. Hence the prior alongshore current jet is too broad, causing v to be overpredicted at the innermost sensor. Similarly, the offshore face of the inner bar is too shallow in the prior, causing increased wave breaking and hence underprediction of H_{mo} at nearby locations (e.g., compare wave transformation from

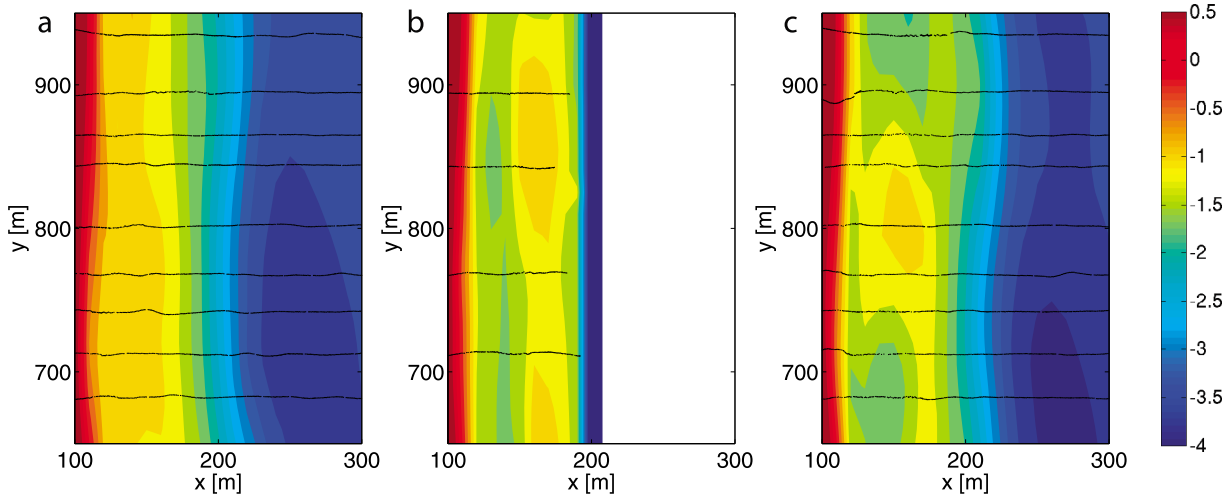

Figure 4. Black is the bathymetric transects collected by CRAB on (a) 18, (b) 20, and (c) 21 October. Colors are the interpolated surveyed bathymetry z_b (hotter colors represent shallower water).

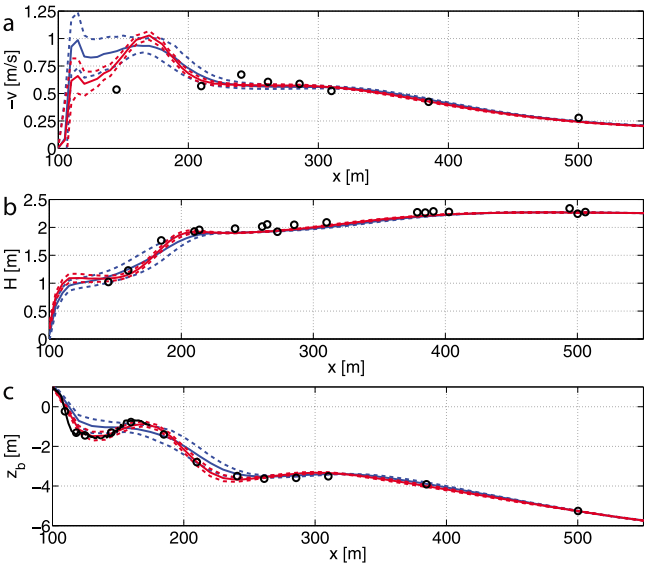

Figure 5. Prior (blue), posterior (red), and measured (black) data for 1-DH case study, 20 October 1130 EST. Dashed lines represent ±1 standard deviation. Black circles correspond to data from fixed instruments (SPUV); black line is CRAB transect collected at $y = 843$ m, on 20 October, 1036–1040 EST. Still water level was 1.16 m NGVD.

$x = 210$ m to $x = 185$ m). After assimilating data, the above errors are reduced and the overall fit is improved, including the fit to h (which was not assimilated).

[48] In order to understand how equation (3) used the observed model data misfit ($d - Lv^f$) to update the full model state ψ, it is useful to examine the coefficient matrix $r = C_{\psi\psi} L_a^T$. In the language of data assimilation, r is usually referred to as the matrix of representers. Each column r_k quantifies the sensitivity of the model to a particular observation (the k'th observation). Hence by analyzing these columns, suitably normalized, we can better understand how the overall model corrections are assembled [*Kurapov et al.*, 2009]. Here we will normalize as follows,

$$\hat{r} = r\left(\frac{\sigma_m + \sigma_d}{\sigma_m^2 + \sigma_d^2}\right). \tag{8}$$

This normalization is obtained by taking model and data errors to be equal to their standard deviations (denoted σ_m and σ_d, respectively), and assuming an isolated observation. We will interpret maps of $\hat{r}$ as the "potential correction" which can be obtained by assimilating a particular measurement. For instance, we will write $\hat{r}_{hv}$ as the potential correction to bathymetry h from assimilating velocity v. In this way, we may compare the magnitude and spatial pattern of the correction derived from each element in the measurement array. Note this analysis is performed without reference to the actual measurements; r is a property of the model (and prior statistics) only. We have also compared equation (8) to the contributions of actual measurements to the overall model update in equation (3), and generally find good agreement.

[49] Figure 6 shows scaled representers for each instrument on the observational transect (including instruments which were not functioning at 1130 EST). Both observation types show the largest potential corrections coming from sensors in the inner surf zone ($x < 250$ m). Potential corrections from outer surf zone sensors are small, because of small prior uncertainty (cf. Figure 5) and/or lack of bathymetric sensitivity at those locations. Hereafter, we will concentrate on the inner surf zone.

[50] Focusing first on $\hat{r}_{hH}$, underprediction of H_{mo} typically resulted in a local increase (deepening) of h; that is, $\hat{r}_{hH}$ is locally-positive. This agrees with the expectation based on saturated depth-limited breaking, $H_{\mathrm{mo}} = \gamma h$, with $\gamma > 0$ (i.e., $\partial H_{\mathrm{mo}}/\partial h > 0$). To be more precise, consider the following local approximation of C_{Hh} near the point x_0:

$$\begin{aligned} C_{Hh} &= E[\delta H_{\mathrm{mo}} \delta h] \\ &\approx E\left[\left(\frac{\delta H_{\mathrm{mo}}}{\delta h}\right)|_{x_0} \delta h \delta h\right] \\ &= \left(\frac{\delta H_{\mathrm{mo}}}{\delta h}\right)|_{x_0} C_{hh}, \end{aligned} \tag{9}$$

where E is expected value, and $\delta H_{\mathrm{mo}}/\delta h$ denotes the relative increment of H_{mo} or a given increment of h, evaluated based on the prior statistics at a given point. As suggested above, the prior statistics for the present case indeed gave $\delta H_{\mathrm{mo}}/\delta h > 0$ for locations where waves were breaking; in fact, $\delta H_{\mathrm{mo}}/\delta h$ was significantly correlated with the prior wave dissipation ($r = 0.58$, $p = 10^{-10}$). Positive $\delta H_{\mathrm{mo}}/\delta h$ occurred in the inner surf zone where dissipation was large, while small (or even negative) $\delta H_{\mathrm{mo}}/\delta h$ occurred outside the surf zone and in reshoaling regions. At locations near the maxima of wave dissipation, $\delta H_{\mathrm{mo}}/\delta h$ had a value of approximately 0.5.

[51] Turning next to $\hat{r}_{hv}$, we note that an underprediction of $-v$ in the prior (i.e., prior predicted current not as large as observed current toward the south, or negative y, direction) always produces a local decrease (shoaling) of h; that is, $-\hat{r}_{hv}$ is locally negative. Conceptually, this behavior is due to the fact that local maxima in $|v|$ tend to be associated with local minima in depth (e.g., a sandbar). Indeed, the prior statistics for the present case gave $\delta(-v)/\delta h < 0$ for all $x > 105$ m.

[52] The above interpretation highlights the role of the model dynamics for determining the local values of $\delta H_{\mathrm{mo}}/\delta h$ and $\delta v/\delta h$, and hence the magnitudes of the representers themselves. Non-local corrections to bathymetry, on the other hand, are derived from a combination of model dynamics and the assumed prior covariance C_{hh}. In order to judge the balance between these two contributions, we may compare $\hat{r}$ to the approximation based on (9) (dashed lines in Figure 6), which is representative of the contribution of C_{hh} to the nonlocal correction. Clearly, C_{hh} plays an important role in determining the basic structure of $\hat{r}$, and hence the corrections themselves, while model dynamics mainly act to amplify and/or shift that structure. This highlights the importance of choosing appropriate prior statistics, if nonlocal corrections are to be trusted.

[53] Finally, we note there are qualitative differences between the shape and magnitude of $\hat{r}_{hv}$ and $\hat{r}_{hH}$, suggesting v and H_{mo} play different roles in the overall correction. To further illustrate this fact, Figure 7 shows the posterior

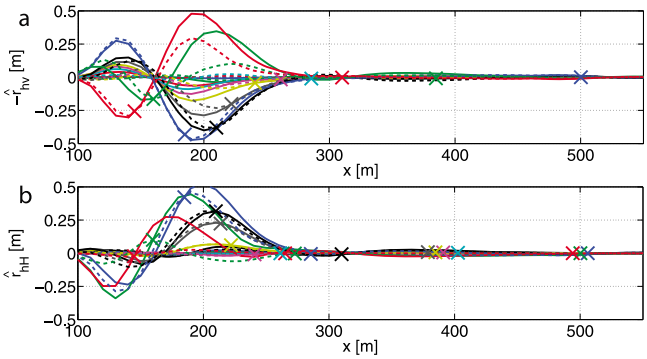

Figure 6. Solid lines are scaled representers. Dashed lines are corresponding approximation based on extrapolation with C_{hh} (see text). Crosses indicate location of measurement for each representer. The $\hat{r}_{hv}$ has been negated for comparison with Figure 5.

model state when each observation type (either v or H_{mo}) is assimilated individually. The results are best understood by considering differences in the posterior H_{mo}. When assimilating v only, the spatial gradient of H_{mo} is altered in the inner surf zone, resulting in a correction to the wave-induced forcing (not plotted); however, the resulting H_{mo} is not in good agreement with observations (in particular, the posterior breakpoint is too far offshore). Conversely, when assimilating H_{mo} only, the magnitude of H_{mo} is improved but the resulting change in wave-induced forcing does not lead to an improved v (particularly at the innermost sensor). Assimilating v and H_{mo} together allows the forcing to be corrected without severely affecting the accuracy of H_{mo}, resulting in an improved overall agreement for all variables (also see section 4.4). The representers (Figure 8) confirm the above interpretation: for the most-shoreward sensors, $\hat{r}_{HH}$ and $\hat{r}_{Hv}$ indicate controls on magnitude and gradient, respectively. That is, the most-shoreward observation points correspond to antinodes of $\hat{r}_{HH}$, and nodes of $\hat{r}_{Hv}$. These sensors dominate the overall correction, producing the above behavior. Further-offshore sensors do not show such a clear contrast between $\hat{r}_{HH}$ and $\hat{r}_{Hv}$, likely due to differences in the qualitative dynamics (e.g., the influence of momentum mixing).

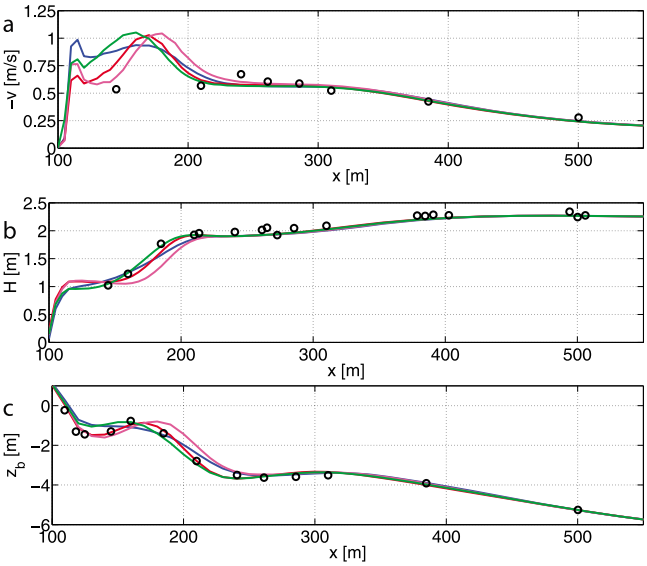

Figure 7. Prior (blue), measured (black), and posterior data when assimilating H_{mo} only (green), v only (magenta), or both (red).

4.3. Assimilation During 2-DH Flow

[54] Having established the conceptual framework for assimilation under simple 1-DH dynamics, we now move to a 2-DH case: 20 October, 1530 EST.

[55] Figure 9 shows the prior prediction of v and H_{mo}. Recall this corresponds essentially to a forward model run, with bathymetry derived from a smoothed interpolation in EOF space (section 3.2). The predictions in the outer surf zone are fairly consistent with observations (overprediction of offshore wave height is likely due to error in the offshore boundary conditions). For sensors in the inner surf zone, $x <$ 250 m, however, the flow becomes alongshore-nonuniform, and the velocity predictions are highly inaccurate in magnitude and even wrong in direction (see sensors at $y \approx 830$ m and $y \approx 700$ m). Given the known bathymetric sampling issues (see section 4.1), we will now explore the possibility that the model error is due to mis-specification of h.

[56] Figure 10 compares the posterior velocity field to observations, after assimilating H_{mo} (46 observations) and v (29 observations). Model data agreement in alongshore current is improved, particularly in the inner surf zone, which is to be expected because that data was assimilated. Importantly, the modeled across-shore currents u are also improved, which can be interpreted as a cross-validation for the update step (u was not assimilated).

[57] The posterior bathymetry is also an improvement over the prior. Figure 11 shows an across-shore transect comparing the prior and posterior h to that measured by the sonar altimeters (again, these measurements were not assimilated). The comparison shows that the update step correctly adjusted the prior in the direction of the actual (measured) bathymetry. As in the 1-DH case study, major corrections occurred in the inner surf zone, whereas outer surf zone ($x >$ 250 m) corrections were relatively small.

[58] Next, as in the 1-DH case study, we examine the scaled representers $\hat{r}$ for 2-DH flow. Figure 12 (top) shows

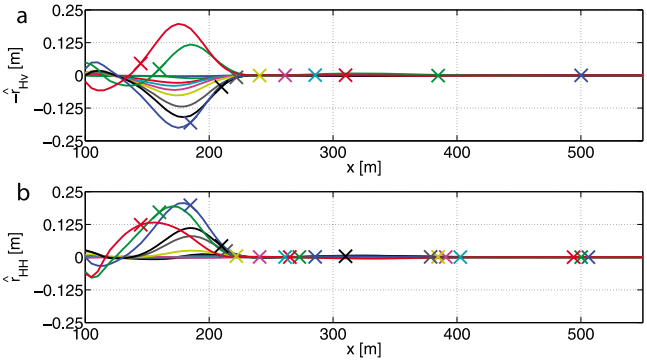

Figure 8. Scaled representers for correction of H_{mo}. Crosses indicate location of measurement for each representer. The $\hat{r}_{Hv}$ has been negated for comparison with Figure 5.

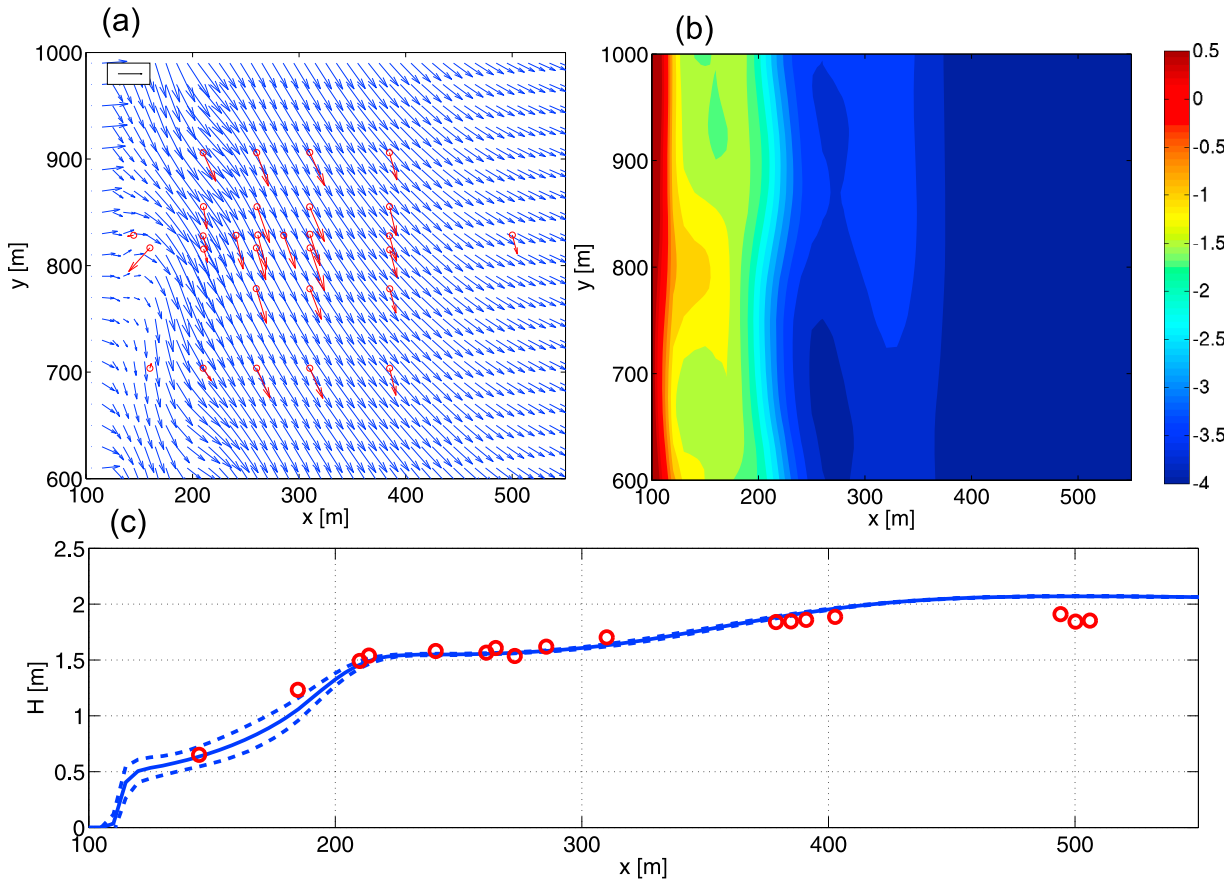

Figure 9. Prior mean velocity, bathymetry, and wave height on transect $y = 828$ m, for 20 October, 1530 EST. (a) Red arrows are observed velocity; blue arrows are modeled velocity, plotted at even grid points; scale arrow in top left is 50 cm/s. (b) Colors are model z_b (still water level was 0.17 m NGVD). (c) Solid and dashed lines are prior mean and standard deviation of H_{mo}, and red circles are measured H_{mo}.

maps from $\hat{r}_{hH}$, the potential correction to h from assimilating measurements of H_{mo}, at four different locations ranging from the inner to outer surf zone. Clearly, H_{mo} is effective for constraining local bathymetry in the inner surf zone, where wave height is strongly controlled by water depth because of depth-limited wave breaking. For measurements in the outer surf zone, $\hat{r}_{hH}$ is much smaller in magnitude, indicating a smaller potential for correction in that region.

[59] Figure 12 (bottom) shows maps from $\hat{r}_{hv}$, the potential corrections to h from observing v. A distinguishing feature of $\hat{r}_{hv}$ in this case is that sensors offshore of the inner bar contribute information about bathymetry onshore of the inner bar. This did not occur under 1-DH dynamics, and hence is attributed to advection by 2-DH currents. This also means a greater number of sensors for v could provide significant (potential) corrections to h: 19 columns of $\hat{r}_{hv}$ had maximum magnitude exceeding 10 cm, as opposed to only six for $\hat{r}_{hH}$. The actual model corrections when assimilating data reflect the same trend: five observations of v contributed corrections of more than 10 cm to h, compared to two for H_{mo}. Thus, the v array included a greater number of "useful" sensors. The corresponding correction to h should be considered more stable, in the sense that it is more robust against isolated observation errors dominating the overall correction. A more rigorous way to examine the stability of the measurement array is to compute the singular value decomposition of the matrices Lr_{hv} and Lr_{hH} (so-called "array-mode analysis," [*Bennett*, 2002; *Kurapov et al.*, 2009]). Five of the singular values for Lr_{hv} exceeded the observational noise level, indicating stable array modes; two singular values for Lr_{hH} passed the same criteria. Thus, again, v was the more stable observation type for the present case.

4.4. Skill Statistics

[60] Next, we evaluate the skill of the posterior model state, compared to that of the prior. Our aim is to quantify the improvement in the model state when assimilating observations of H_{mo} and v, together as well as individually. Here we will limit our discussion to the inner surf zone region $x < 250$ m, for two reasons: first, as noted earlier, corrections were broadly confined to this region, whereas the outer surf zone was constrained by low prior uncertainty; second, the point $x = 250$ m corresponds to a minimum in modeled wave dissipation, separating two distinct wave breaking regions and flow regimes. For completeness, skill statistics for $x > 250$ m are listed in Table B1. Indeed, the model updates in that region were small, for the reasons stated above, and often did not result in an improved fit to cross-validation variables.

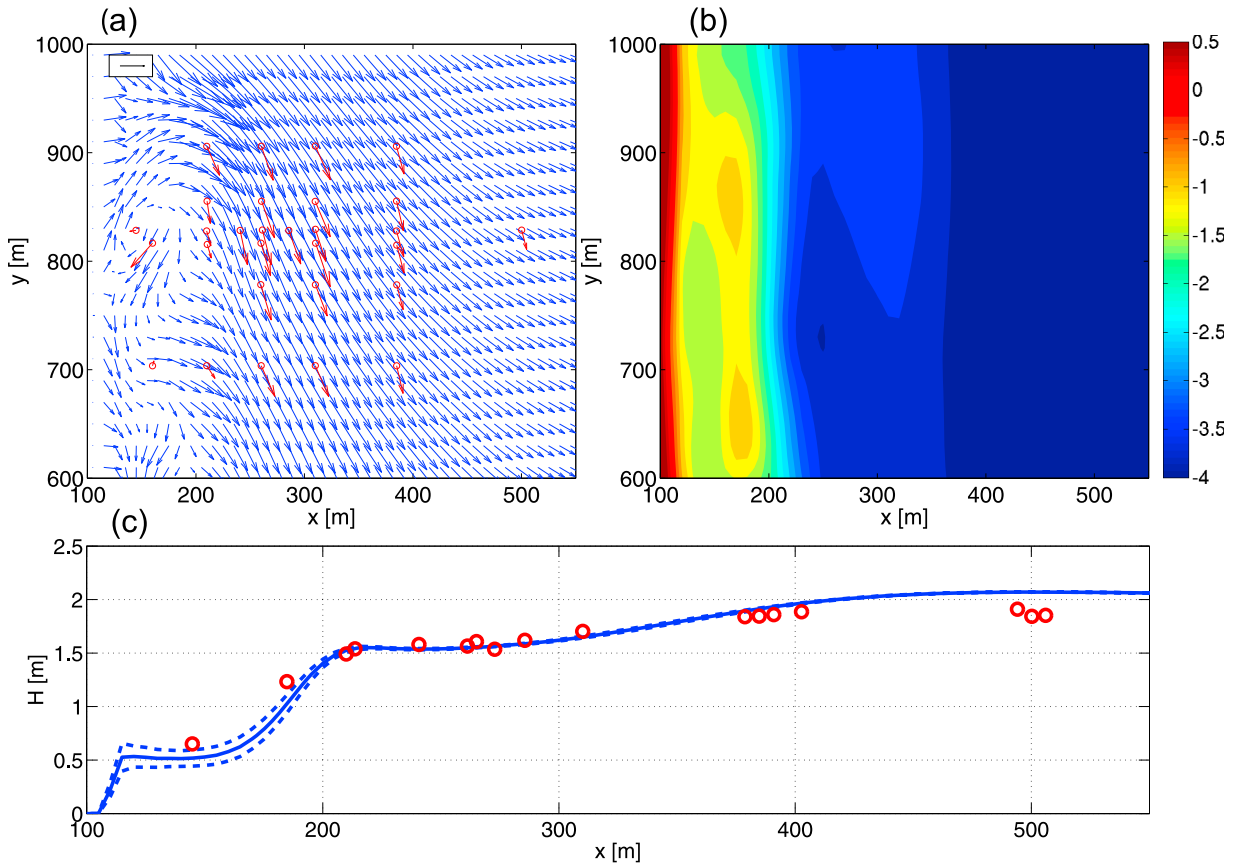

Figure 10. As in Figure 9 but for posterior (updated) fields.

[61] The skill of the prior and posterior model states will be assessed in a probabilistic validation framework [*Casati et al.*, 2008], taking into account the predicted model state ψ as well as the predicted uncertainty $C_{\psi\psi}$. Specifically, we adopt the Continuous Ranked Probability Score (CRPS; Appendix A) to assess skill, which measures the overall difference between prediction and observation probability density functions. In the limit of deterministic predictions and observations, CRPS is equal to the root-mean square (rms) error. We also compute a skill score,

$$S = 1 - (CRPS)_a/(CRPS)_f, \tag{10}$$

which indicates whether the posterior state (subscript a) has improved skill relative to the prior (subscript f). Finally, for completeness, we also report the RMS error, as a simple and easy to understand measure of accuracy which does not take into account the predicted uncertainty. These statistics are given in Table 1, and the results are discussed next.

5. Discussion

5.1. Assimilation Skill

[62] Table 1 reports statistics which assess the improvement in model skill when assimilating different combinations of data. In general, if the present methodology is skillful, we should find a decrease in RMS error and CRPS (i.e., positive skill score S) as a result of assimilating data. When this is not the case, we will generally assume the inversion is converging (with respect to increasing number of observations) on an incorrect posterior state ψ. In this section, we ask: what data were required to obtain a skillful inverse, in the above sense?

[63] First, we consider the case where both v and H_{mo} are assimilated, under 2-DH dynamics (20 October, 1530 EST). The resulting posterior state is improved in all variables, including the cross-validation variables u and h. This indicates the assimilation of data has introduced a realistic correction to the overall model state. The error that remains in the posterior estimate represents a combination of still-unresolved uncertainty in the input h, observational/representation errors, and (importantly) errors due to model physics.

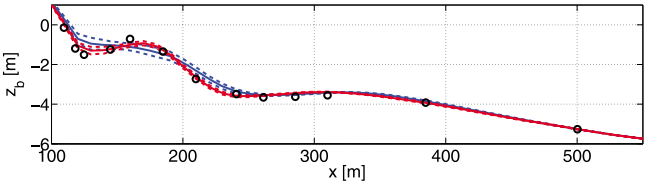

Figure 11. Across-shore transect (y = 828 m) of prior (blue), posterior (red), and measured (black) z_b (still water level was 0.17 m NGVD). Dashed lines represent ±1 standard deviation.

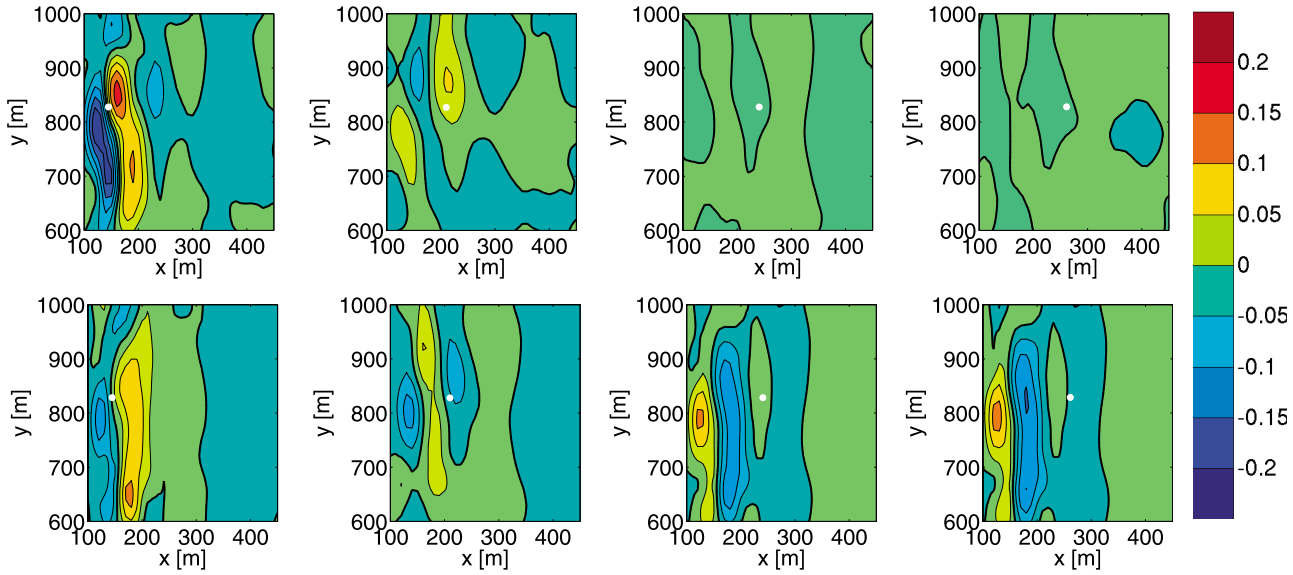

Figure 12. Maps from scaled representer submatrix (top) $\hat{r}_{hH}$ and (bottom) $\hat{r}_{hv}$, for select measurement locations (white dots). Thick black contour is 0 cm, and subsequent contours are plotted at 5 cm intervals.

[64] When only v is assimilated (2-DH case), the situation is quite different. Both u and v are brought into good agreement with the observations, and CRPS indicates positive skill. The prediction for h is also improved, although not to the extent as when H_{mo} and v were assimilated together. However, the posterior H_{mo} is actually less accurate than the prior, and has larger CRPS, indicating the assimilation is not converging toward the true H_{mo}. Overall, cross validation suggests the assimilation is overfitting the velocity data, at the expense of H_{mo} (we define overfitting, here, as achieving improved skill in one variable, at the expense of any other variable).

[65] When only H_{mo} is assimilated (2-DH case), we find a similar result to when only v was assimilated. The posterior state is an improved fit to the assimilated variable, but not to the unassimilated variables (in this case, the skill for u, v and h is essentially unchanged). Again, the result may be converging on an incorrect posterior model state.

[66] Statistics from the 1-DH case (20 October, 1130 EST) indicate similar results, with overfitting occurring unless H_{mo} and v are assimilated together. One distinction between the 1-DH and 2-DH cases lies in their ability to correct the across-shore current u. In the 2-DH case, u was improved when v was assimilated, but made worse when H_{mo} was assimilated; the opposite was true for the 1-DH case. This is perhaps not surprising: under 1-DH dynamics, u is entirely due to the below-trough return flow of wave volume flux, which is in turn directly related to H_{mo}. In contrast, in the 2-DH case, the cross-shore current is likely driven as a result of nonlocal alongshore-nonuniform dynamics. Another distinction between the 1-DH and 2-DH results is that, in the 1-DH case, h could be better corrected by assimilation of H_{mo} than by assimilation of v. We note, however, that the 1-DH case had only three active sensors for v in the inner surf zone, compared to six active sensors for H_{mo}.

[67] A result common to both 1-DH and 2-DH cases is that the true ocean state ψ can only be recovered by assimilating both variables v and H_{mo}. This may be partly attributed to the fact v and H_{mo} provide different (complimentary) information with regard to the dynamics, as demonstrated using the 1-DH model in section 4.2. However, other factors may serve to exacerbate the overfitting behavior. For instance, we have already noted that the specified prior C_{hh} influences the shape of representers, and hence the correction itself; errors in this specification could lead to unexpected results. Errors may also exist in the forward model, causing the true v and H_{mo} to be incompatible under the "perfect model" assumption; *Plant et al.* [2009] find an analogous result, where artificial smoothing of bathymetry leads to decreased error in H_{mo} but increased error in v. One way to exclude the influence of the above effects is to extract synthetic observations from a forward model run with idealized bathymetry. From that experiment, we find a similar result as above: assimilating v appears to correct the gradient of H_{mo}, and hence the wave-induced forcing, while the magnitude of H_{mo} is not improved (and vice versa). However, the synthetic tests do not show strongly-negative skill in the unassimilated variable as was the case with real observations. Hence, we cannot not rule out the possibility of model error being present.

[68] To summarize, the ensemble-based method was successful in assimilating observations and correcting bathymetry, when using all of the available data for v and H_{mo}. The resulting prediction is an improvement over the prior (rms error and CRPS are both decreased). When one observation type (either v or H_{mo}) was withheld, bathymetry could still be improved relative to the prior, but only at the expense of a poor posterior prediction of the unassimilated variable (either H_{mo} or v). This is explained by considering the complimentary information carried by each variable, although other factors are considered. In any case, there is an inherent benefit of assimilating (semi)independent data types.

Table 1. Model Accuracy Statistics Before and After Assimilation for Sensors in $x < 250$ m[a]

Variable(s) Assimilated	Variable Updated	Units	1-DH (1130 EST)			2-DH (1530 EST)		
			ε	*CRPS*	*S*	ε	*CRPS*	*S*
None (prior)	u	m/s	0.13	0.13	–	0.33	0.68	–
	v	m/s	0.22	0.24	–	0.29	0.56	–
	H_{mo}	m	0.11	0.11	–	0.11	0.18	–
	h	m	0.45	0.75	–	0.41	0.88	–
H_{mo}, v	u	m/s	0.13	0.16	–0.17	0.19	0.36	0.48
	v	m/s	0.15	0.18	0.27	0.054	0.055	0.90
	H_{mo}	m	0.080	0.092	0.16	0.084	0.15	0.18
	h	m	0.20	0.28	0.63	0.18	0.30	0.66
H_{mo}	u	m/s	0.11	0.12	0.11	0.30	0.62	0.093
	v	m/s	0.26	0.35	–0.47	0.28	0.55	0.013
	H_{mo}	m	0.041	0.033	0.70	0.064	0.10	0.46
	h	m	0.36	0.61	0.18	0.37	0.83	0.061
v	u	m/s	0.17	0.21	−0.54	0.20	0.36	0.48
	v	m/s	0.12	0.11	0.52	0.054	0.053	0.90
	H_{mo}	m	0.19	0.30	–1.7	0.13	0.25	–0.34
	h	m	0.42	0.74	0.016	0.20	0.32	0.64

[a]Here ε is RMS difference between model and observations, CRPS is the continuous ranked probability score (see text and Appendix A), and *S* is a skill score (equation (10)). The calculation of CRPS for u and h assume observational error standard deviations of 6.7 cm/s (same as for v) and 10 cm, respectively.

5.2. Bathymetric Input Sensitivity

[69] In sections 4.2 and 4.3, representers were used to clarify how prior error/sensitivity is utilized for the assimilation of data: by combining all of the representers (with appropriate normalization), one obtains the posterior model state. The magnitude of the potential correction fields $\hat{r}$ indicate strong model sensitivity between the observed variables v and H_{mo} and the target variable h.

[70] A closely-related problem is the extent to which v and H_{mo} are sensitive to errors in h. A direct quantification of this sensitivity is given by the prior standard deviation of modeled v and H_{mo}, which, for October 1530 EST, had maximum values of 31 cm/s and 19 cm, respectively. At the observation locations, prior standard deviations ranged from 0–29 cm/s (for v), and 0–10 cm (for H_{mo}), with larger values occurring closer to shore. The 1-DH case (20 October, 1130 EST) gave similar values, except for v at the observation locations which ranged from 0–13 cm/s. Given that model validation studies have reported errors on these same orders of magnitude [e.g., *Ruessink et al.*, 2001], this suggests bathymetric input error may be equally as important as process error, for cases like the ones we consider here.

[71] It should be noted, however, that the above results are influenced by the specified prior statistics for h. In particular, the uncertainty in h is constructed, here, to reflect unresolved changes in bathymetry between surveys. Other sources of uncertainty, such as instrument error or spatial over-smoothing [*Plant et al.*, 2009], could be treated by a similar analysis, with C_{hh} redefined appropriately.

5.3. Effect of Sampling Scheme

[72] In the preceding sections, we have performed the model inverse using all available measurements. However, the present data set, from the SD97 experiment, had an unusually large observational array which sampled both alongshore and across-shore variability. Previous experiments such as SuperDuck [*Oltman-Shay and Howd*, 1989] and DUCK94 [*Elgar et al.*, 1997; *Feddersen and Guza*, 1998; *Gallagher et al.*, 1998] have focused on only alongshore or across-shore variability, respectively. It is natural to ask whether the present method can be applied under a more limited experimental layout.

[73] Figures 13 and 14 show the posterior wave and current fields for October 20, 1530 EST (cf. Figure 10), obtained by assimilating v and H_{mo} from a single alongshore or across-shore transect. The sampling schemes are similar to SuperDuck and DUCK94, respectively. We find that, in the present case, either sampling scheme is sufficient to improve the prediction of the model state (a positive skill score *S* is found for all variables). However, the posterior bathymetry is more accurate when using the alongshore array (skill $S = 0.77$, RMS error $\varepsilon = 15$ cm, taking measurements from $x < 250$ m), compared to the across-shore array ($S = 0.45$, $\varepsilon = 26$ cm). On the other hand, the alongshore array was less able to constrain wave height ($S = 0.051$, $\varepsilon = 10$ cm), compared to the across-shore array ($S = 0.27$, $\varepsilon = 8.0$ cm).

5.4. Assimilation of Other Observational Data Types

[74] So far, we have presented results for assimilation of v and H_{mo}, two commonly-measured observational data types. However, standard surf zone instruments are also capable of recovering additional information about the wavefield, including wave directional information. As an example, here we test the assimilation of the radiation stress tensor component S_{xy}.

[75] An observational estimate of S_{xy} can be computed from a cross-spectral analysis of time series of u and v [*Higgins et al.*, 1981]. Here we computed the cross spectrum from 17 min records, using a Bartlett taper. Depth dependence is accounted for using linear wave theory.

[76] *Guza and Thornton* [1978] have noted that S_{xy} is generally a statistically unstable observation which can be very difficult to measure, particularly due to instrument alignment issues. Hence, the choice of observational error for this derived quantity was not obvious, and we chose an error of 20 N/m (in the present test case, S_{xy} varied from −87 to 230 N/m). Values of 15 N/m and 30 N/m were also tested, and did not change the qualitative conclusions that follow.

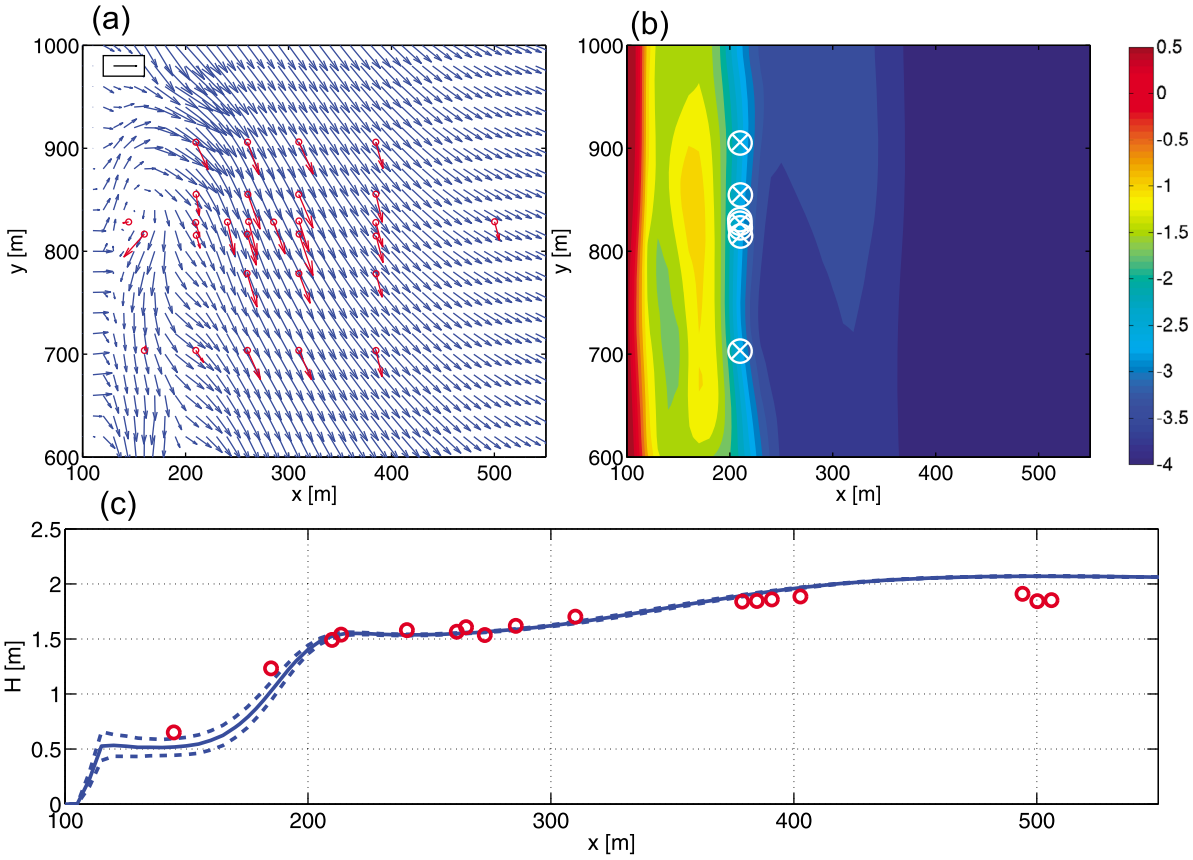

Figure 13. As in Figure 10 but for posterior (updated) fields using alongshore transect sampling scheme. Assimilated observations of v are marked by white crosses, and observations of H_{mo} are marked by white circles.

[77] When S_{xy} is assimilated (alone) for the 20 October 1530 EST case presented in section 4, the effect on the posterior bathymetry is qualitatively similar to that found when assimilating v. Specifically, the areas onshore and offshore of the inner bar at $x \approx 160$ m were made deeper, a correction which could not be attained by assimilating H_{mo} alone. Hence, S_{xy} could be used in conjunction with H_{mo} to generate an improved posterior bathymetry ($S = 0.65$, $\varepsilon = 18$ cm, for $x < 250$ m). On the other hand, assimilation of S_{xy} was not found to be a substitute for the information provided by v. The skill of the posterior v was not much improved by assimilation of S_{xy} ($S = 0.31$, $\varepsilon = 22$ cm/s), compared to when v itself was assimilated. Results were similar for the 1-DH case. In summary, then, S_{xy} appears to provide information about bathymetry, but further work would be required to incorporate this data type into an accurate assimilation.

6. Conclusions

[78] In this study, we have applied standard methods from data assimilation to examine the sensitivity of surf zone models to bathymetric uncertainty. Our purpose was two-fold: to directly analyze the impact of bathymetric uncertainty on a surf zone model using field data and to demonstrate the potential of ensemble-based data assimilation for 2-DH nearshore prediction.

[79] The results presented here show that, even in an extensively-sampled experimental setting (SD97, possibly the most detailed short-term bathymetric data set available to date), bathymetric uncertainty can play a leading role in determining the error of hindcast model circulation. This was demonstrated in several ways, as described below.

[80] Figures 5 and 9 illustrate that the best prior estimate of bathymetry can lead to poor model results in the inner surf zone for a particular field case. On its face, this could indicate a problem with model physics, or a problem with model inputs. However, by assimilating data under the assumption of perfect model physics and uncertain bathymetry, we were able to derive a consistent model state. Thus, we conclude that the standard approach of estimating bathymetry from recent bathymetric surveys and running the forward model did not apply here, as the bathymetry was changing rapidly (timescales of hours to days) and was therefore very uncertain.

[81] The underlying details of the assimilation step were investigated using an analysis of the matrix of representers [*Kurapov et al.*, 2009], i.e., the interrelationship (covariance) between the modeled H_{mo}, v, and h. We found that surf zone H_{mo} tended to provide slightly larger magnitudes of correction to h, but corrections were relatively localized in space. Under 2-DH flow, observations of v could provide nonlocal corrections to h, which meant a larger portion of the observational array for v was useful for the assimilation.

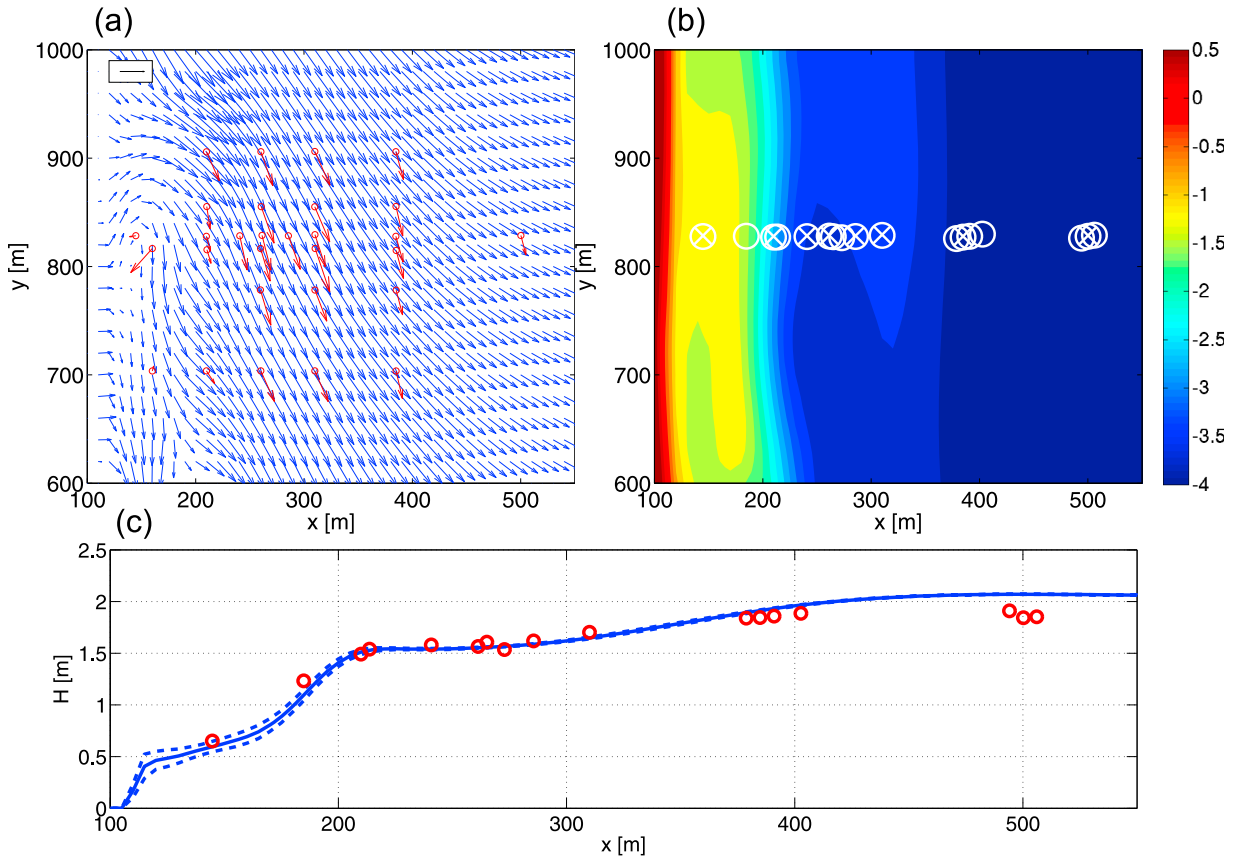

Figure 14. As in Figure 13 but for across-shore sampling scheme.

The pattern and magnitude of the corrections are determined by a combination of C_{hh} (which must be specified) and the model dynamics. In this case, C_{hh} represents the estimated variability in h due to unresolved bathymetric change through time.

[82] Table 1 reports the model-data misfit before and after assimilating data. For 2-DH (1-DH) flow, root-mean square errors in v and H_{mo} in the inner surf zone were reduced by 81% (27%) and 24% (27%), respectively. Errors in h and u, variables which were not assimilated, were also reduced, by 56% (56%) and 42% (0%), respectively. Thus a significant portion of model output errors were linked to input (bathymetric) errors in a self-consistent way. However, we also found the assimilation to be sensitive to the type of observations used: only by assimilating multiple observation types (v and H_{mo} together) were we able to avoid overfitting the data. This was explained by considering the different types of information carried by each variable: observations of v were useful for constraining gradients of H_{mo}, but not magnitudes, and vice versa for H_{mo}.

[83] The above results all point to a strong model sensitivity to the input h; this sensitivity was quantified directly using the prior ensemble variance. The estimated uncertainty in v and H_{mo} due to uncertainty in h was found to be up to 29 cm/s and 10 cm, respectively, at the measurement locations. These values are comparable to what is reported in typical field validation studies (e.g., [*Ruessink et al.*, 2001]). We stress, however, the modeled uncertainty is conditioned by the (specified) uncertainty in h.

[84] Finally, we have tested the above results when using a subset of the available measurements. It was shown that an accurate posterior bathymetry and velocity field can be obtained when using only a single alongshore array of sensors, noting the present situation had strongly 2-DH flow and therefore this configuration provides nonredundant information. An across-shore array gave a less skillful posterior estimate of bathymetry and velocity, but was necessary for an accurate estimate of wave height.

[85] Based on the above results, we conclude 2-DH velocity and wave height observations do provide information about surf zone bathymetry, which can be exploited using statistical methods. Conversely, uncertainty in bathymetry (which is often large due to sampling constraints) can have a strong impact on model skill, a fact which should be considered when validating models.

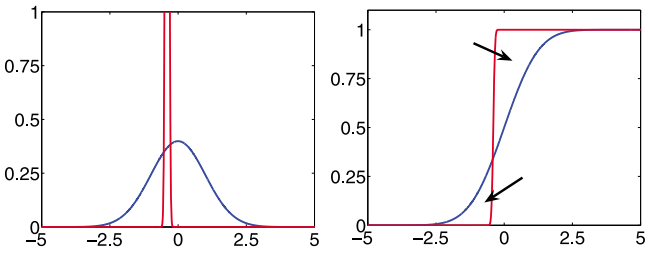

Figure A1. The (left) pdf and (right) cdf representations of the prediction (blue) and observation (red).

Table B1. As in Table 1 but for $x > 250$ m

Variable(s) Assimilated	Variable Updated	Units	1-DH (1130 EST)			2-DH (1530 EST)		
			ε	*CRPS*	*S*	ε	*CRPS*	*S*
None (prior)	u	m/s	0.19	0.34	–	0.15	0.48	–
	v	m/s	0.032	0.042	–	0.14	0.42	–
	H_{mo}	m	0.075	0.17	–	0.11	0.44	–
	h	m	0.091	0.085	–	0.12	0.23	–
H_{mo}, v	u	m/s	0.20	0.35	–0.029	0.16	0.53	–0.11
	v	m/s	0.028	0.044	–0.049	0.091	0.26	0.37
	H_{mo}	m	0.068	0.15	0.10	0.11	0.44	–0.0077
	h	m	0.13	0.16	–0.86	0.14	0.32	–0.38
H_{mo}	u	m/s	0.19	0.35	–0.017	0.15	0.50	–0.048
	v	m/s	0.030	0.046	–0.098	0.16	0.50	–0.20
	H_{mo}	m	0.070	0.16	0.077	0.11	0.44	–0.0015
	h	m	0.11	0.12	–0.37	0.11	0.22	0.065
v	u	m/s	0.19	0.34	–0.014	0.16	0.51	–0.079
	v	m/s	0.028	0.042	0.0044	0.084	0.24	0.43
	H_{mo}	m	0.073	0.16	0.032	0.11	0.44	–0.0098
	h	m	0.12	0.13	–0.58	0.15	0.36	–0.53

Appendix A: Continuous Ranked Probability Score

[86] In section 4.4, we test the skill of the prior and posterior estimates of the ocean state ψ, by cross-validation with observations. This involves testing the accuracy of the ocean state prediction, as well as the predicted uncertainty. Both must be assessed together in order to fully characterize the skill of the assimilation methodology. The validation is carried out using the Continuous Ranked Probability Score (CRPS), defined below.

[87] For a given probabilistic forecast of a scalar random variable x (e.g., the prior or posterior model state ψ and its uncertainty $C_{\psi\psi}$), define the cumulative distribution function (cdf) $f_X(x)$. Also define the cdf of the same random variable x as determined from an observation of the same variable, $f_Y(x)$. Then the CRPS is defined by *Hersbach* [2000]; *Gneiting et al.* [2008]; *Casati et al.* [2008]

$$CRPS = \int_{-\infty}^{\infty} (f_X(x) - f_Y(x))^2 dx. \tag{A1}$$

Note this is a generalization of the standard definition, allowing for observational uncertainty (e.g., instrument error).

[88] Figure A1 shows a graphical interpretation of the CRPS, as the squared area of the regions pointed to by the arrows. When the probability density functions (pdf's) of the prediction and the observation coincide, the CRPS goes to zero; large values of CRPS indicate an unskilled prediction. Note that CRPS takes into account both calibration (the agreement of the predicted and observed expected value) and sharpness (the agreement of the predicted and observed uncertainty). The prediction depicted in Figure A1 is fairly well calibrated, but is not particularly sharp.

[89] The extension to multiple observations (vector-valued random variables x) follows *Gneiting et al.* [2008], who point out the following identity (from *Baringhous and Franz* [2004], Lemma 2.2):

$$CRPS = E[\| X - Y \|] - \frac{1}{2}E[\| X - X' \|] - \frac{1}{2}E[\| Y - Y' \|] \geq 0, \tag{A2}$$

where X and X' are independent realizations following the cdf f_X (similar for Y and Y'), $\| \cdot \|$ is the Euclidean norm, and E denotes expected value (computed herein using Monte-Carlo methods). With the norm thus defined, CRPS is naturally extended for any number of observations. This definition also means CRPS reduces to the RMS error when the variables are deterministic.

Appendix B: Skill Statistics for $x > 250$ m

[90] For completeness, Table B1 lists model skill for the offshore sensors $x > 250$ m (discussed briefly in section 4.4).

[91] **Acknowledgments.** We wish to thank the COAS coastal modeling group and especially A. Kurapov for useful discussions and insights on this topic. The anonymous reviewers also provided excellent comments and suggestions. This work was supported by the Office of Naval Research grants N00014-02-1-0198, N00014-07-1-0852, and N00014-09-1-0121.

References

Aarninkhof, S. G., B. G. Ruessink, and J. A. Roelvink (2005), Nearshore subtidal bathymetry from time-exposure video images, *J. Geophys. Res.*, *110*, C06011, doi:10.1029/2004JC002791.

Baringhous, L., and C. Franz (2004), On a new multivariate two-sample test, *J. Multi. Anal.*, *88*, 190–206.

Bennett, A. F. (2002), *Inverse Modeling of the Ocean and Atmosphere*, Cambridge Univ. Press, New York.

Birkemeier, W. A. (1984), The crab: A unique nearshore surveying vehicle, *J. Surv. Eng.*, *110*(1), 1–7.

Booij, N., R. C. Ris, and L. H. Holthuijsen (1999), A third-generation wave model for coastal regions: 1. Model description and validation, *J. Geophys. Res.*, *104*(C4), 7649–7666, doi:10.1029/1998JC900123.

Bowen, A., and R. Holman (1989), Shear instabilities of the mean longshore current, *J. Geophys. Res.*, *94*(C12), 18,023–18,030, doi:10.1029/JC094iC12p18023.

Casati, B., D. Stephenson, P. Nurmi, A. Ghelli, M. Pocernich, U. Damrath, E. Ebert, B. Brown, and S. Mason (2008), Forecast verification: Current status and future directions, *Meteorol. Appl.*, *15*, 3–18.

Catalan, P., and M. Haller (2007), Remote sensing of breaking wave phase speeds with application to nonlinear depth inversions, *Coastal Eng.*, *55*, 93–111.

Elgar, S., R. T. Guza, B. Raubenheimer, T. H. Herbers, and E. L. Gallagher (1997), Spectral evolution of shoaling and breaking waves on a barred beach, *J. Geophys. Res.*, *102*(C7), 15,797–15,805, doi:10.1029/97JC01010.

Elgar, S., R. T. Guza, W. C. O'Reilly, B. Raubenheimer, and T. H. Herbers (2001), Wave energy and direction observed near a pier, *J. Waterw. Port Coastal Ocean Eng.*, *207*(1), 2–6.

Evensen, G. (2006), *Data Assimilation: The Ensemble Kalman Filter*, Springer, New York.
Feddersen, F., and R. T. Guza (1998), Alongshore momentum balances in the nearshore, *J. Geophys. Res.*, *103*(C8), 15,667–15,676, doi:10.1029/98JC01270.
Feddersen, F., and R. T. Guza (2003), Observations of nearshore circulation: Alongshore uniformity, *J. Geophys. Res.*, *108*(C1), 3006, doi:10.1029/2001JC001293.
Feddersen, F., R. T. Guza, and S. Elgar (2004), Inverse modeling of one-dimensional setup and alongshore current in the nearshore, *J. Phys. Oceanogr.*, *34*, 920–933.
Gallagher, E., S. Elgar, and R. Guza (1998), Observations of sandbar evolution on a natural beach, *J. Geophys. Res.*, *103*(C2), 3203–3215, doi:10.1029/97JC02765.
Gneiting, T., L. Stanberry, E. Grimit, L. Held, and N. Johnson (2008), Assessing probabilistic forecasts of multivariate quantities, with an application to ensemble predictions of surface winds, *Test*, *17*, 211–235.
Guza, R., and E. Thornton (1978), Variability of longshore currents, in *Proceedings of 16th International Coastal Engineering Conference*, pp. 756–775, Am. Soc. Civ. Eng., New York.
Haas, K. A., I. A. Svendsen, M. C. Haller, and Q. Zhao (2003), Quasi-three-dimensional modeling of rip current systems, *J. Geophys. Res.*, *108*(C7), 3217, doi:10.1029/2002JC001355.
Hersbach, H. (2000), Decomposition of the continuous ranked probability score for ensemble prediction systems, *Weather Forecast.*, *15*(5), 559–570.
Higgins, A. L., R. J. Seymour, and S. S. Pawka (1981), A compact representation of ocean wave directionality, *Appl. Ocean Res.*, *3*, 105–112.
Hsu, Y. L., J. D. Dykes, and R. A. Allard (2006), Evaluation of Delft3D performance in nearshore flows, *Tech. Rep. NRL/MR/7320–06-8984*, Nav. Res. Lab., Stennis Space Center, Miss.
Kuik, A. H., G. P. van Vledder, and L. H. Holthuijsen (1988), A method for the routine analysis of pitch-and-roll buoy wave data, *J. Phys. Oceanogr.*, *18*, 1020–1034.
Kurapov, A. L., G. D. Egbert, J. S. Allen, and R. N. Miller (2007), Representer-based variational data assimilation in a nonlinear model of nearshore circulation, *J. Geophys. Res.*, *112*, C11019, doi:10.1029/2007JC004117.
Kurapov, A. L., G. D. Egbert, J. S. Allen, and R. N. Miller (2009), Representer-based analyses in the coastal upwelling system, *Dyn. Atmos. Oceans*, *48*, 198–218.
Long, C. E. (1996), Index and bulk parameters for frequency-directional spectra measured at CERC Field Research Facility, July 1994 to Auguest 1995, *Misc. Pap. CERC-96-6*, U.S. Army Eng. Waterw. Exp. Stn., Vicksburg, Miss.
Longuet-Higgins, M. S. (1970), Longshore currents generated by obliquely incident sea waves, 2, *J. Geophys. Res.*, *75*(33), 6790–6801, doi:10.1029/JC075i033p06790.
Longuet-Higgins, M. S., and R. W. Stewart (1964), Radiation stress in water waves; a physical discussion with applications, *Deep Sea Res.*, *11*, 529–563.
Mei, C. C. (1983), *The Applied Dynamics of Ocean Surface Waves*, Wiley, New York.
Morris, B. J. (2001), Nearshore wave and current dynamics, Ph.D. thesis, Nav. Postgrad. Sch., Monterey, Calif.
Mourre, B., P. D. Mey, F. Lyard, and C. L. Provost (2004), Assimilation of sea level data over continental shelves: An ensemble method for the exploration of model errors due to uncertainties in bathymetry, *Dyn. Atmos. Oceans*, *38*, 93–101.
Oke, P., and P. Sakov (2007), Representation error of oceanic observations for data assimilation, *J. Atmos. Oceanic Techonol.*, *25*, 1004–1017.
Oltman-Shay, J., and P. Howd (1989), Shear instabilities of the mean longshore current: 2. Field observations, *J. Geophys. Res.*, *94*(C12), 18,031–18,042, doi:10.1029/JC094iC12p18031.
Plant, N. G., K. T. Holland, and J. A. Puleo (2002), Analysis on the scale of errors in nearshore bathymetry, *Mar. Geol.*, *191*, 71–86.
Plant, N. G., K. L. Edwards, J. M. Kaihatu, J. Veeramony, L. Hsu, and K. T. Holland (2009), The effect of bathymetric filtering on nearshore process model results, *Coastal Eng.*, *56*, 484–493.
Reniers, A. H., and J. A. Battjes (1997), A laboratory study of longshore currents over barred and nonbarred beaches, *Coastal Eng.*, *30*, 1–22.
Reniers, A. J., J. A. Roelvink, and E. B. Thornton (2004), Morphodynamic modeling of an embayed beach under wave group forcing, *J. Geophys. Res.*, *109*, C01030, doi:10.1029/2002JC001586.
Ruessink, B. G., J. R. Miles, F. Feddersen, R. T. Guza, and S. Elgar (2001), Modeling the alongshore current on barred beaches, *J. Geophys. Res.*, *106*(C10), 22,451–22,463, doi:10.1029/2000JC000766.
Slinn, D. N., P. A. Newberger, and R. A. Holman (1998), Nonlinear shear instabilities of alongshore currents, *J. Geophys. Res.*, *103*(C9), 18,357–18,379, doi:10.1029/98JC01111.
Splinter, K., and R. Holman (2009), Bathymetry estimation from single-frame images of nearshore waves, *IEEE Trans. Geosci. Remote Sens.*, *47*(9), 3151–3160.
Stockdon, H. F., and R. A. Holman (2000), Estimation of wave phase speed and nearshore bathymetry from video imagery, *J. Geophys. Res.*, *105*(C9), 22,015–22,033, doi:10.1029/1999JC000124.
Svendsen, I. A., and U. Putrevu (1994), Nearshore mixing and dispersion, *Proc. R. Soc. London A*, *445*(1925), 561–576.
Svendsen, I. A., K. Haas, and Q. Zhao (2000), Quasi-3D nearshore circulation model, shorecirc, version 1.3.6, technical report, Cent. for Appl. Coastal Res., Univ. of Del., Newark, Del.
Thornton, E. B., and R. T. Guza (1986), Surf zone longshore currents and random waves: Field data and models, *J. Phys. Oceanogr.*, *16*, 1165–1178.
VanDongeren, A., N. Plant, A. Cohen, D. Roelvink, M. C. Haller, and P. Catalan (2008), Beach wizard: Nearshore bathymetry estimation through assimilation of model computations and remote observations, *Coastal Eng.*, *55*, 1016–1027.
Wilson, G. W. (2009), Field validation of a nearshore circulation model for alongshore-nonuniform flows, M.S. thesis, Oreg. State Univ, Corvallis, Oreg.
Zhao, Q., I. Svendsen, and K. Haas (2003), Three-dimensional effects in shear waves, *J. Geophys. Res.*, *108*(C8), 3270, doi:10.1029/2002JC001306.

R. A. Holman, H. T. Özkan-Haller, and G. W. Wilson, College of Oceanic and Atmospheric Sciences, Oregon State University, 104 COAS Administration Bldg., Corvallis, OR 97331, USA. (holman@coas.oregonstate.edu; ozkan@coas.oregonstate.edu; gwilson@coas.oregonstate.edu)